

De-Trending Time Series for Astronomical Variability Surveys

Dae-Won Kim^{1,2,3*}, Pavlos Protopapas^{1,2}, Charles Alcock¹, Yong-Ik Byun³, Federica B. Bianco^{1,4}

¹*Harvard Smithsonian Center for Astrophysics, Cambridge, MA, USA*

²*Initiative in Innovative Computing, Harvard University, Cambridge, MA, USA*

³*Department of Astronomy, Yonsei University, Seoul, Korea*

⁴*Department of Physics and Astronomy, University of Pennsylvania, Philadelphia, PA, USA*

Accepted ???; Received ???

ABSTRACT

We present a de-trending algorithm for the removal of trends in time series. Trends in time series could be caused by various systematic and random noise sources such as cloud passages, changes of airmass, telescope vibration, CCD noise or defects of photometry. Those trends undermine the intrinsic signals of stars and should be removed. We determine the trends from subsets of stars that are highly correlated among themselves. These subsets are selected based on a hierarchical tree clustering algorithm. A bottom-up merging algorithm based on the departure from normal distribution in the correlation is developed to identify subsets, which we call clusters. After identification of clusters, we determine a trend per cluster by weighted sum of normalized light-curves. We then use quadratic programming to de-trend all individual light-curves based on these determined trends. Experimental results with synthetic light-curves containing artificial trends and events are presented. Results from other de-trending methods are also compared. The developed algorithm can be applied to time series for trend removal in both narrow and wide field astronomy.

Key words: methods: data analysis - methods: statistical - methods: miscellaneous - surveys

1 INTRODUCTION

Small-aperture telescopes have detected a large number of exo-planet transits (Alonso et al. 2004; Bakos et al. 2004; McCullough et al. 2005; Bakos et al. 2007; Burke et al. 2008; Pál et al. 2008; Pollacco et al. 2008). A large number of variable stars have also been detected by surveys that use such telescopes (Schmidt 1991; Akerlof et al. 2000; Pojman-ski 2005; Schmidt et al. 2007; Pigulski & Pojmański 2008; Szczygiel & Fabrycky 2008). A weakness in these surveys is that the signal to noise ratio (S/N) is lower than the S/N obtained by larger-aperture telescopes. The low S/N can be attributed not only to the small-aperture size but also to noise in CCD images such as non-uniform illumination, or to local weather changes throughout the field (especially in the case of wide field surveys). To improve the S/N and thus improve the detectability of variability, these noise sources should be minimized.

Some of these noise sources are strongly correlated between light-curves of different stars. For example, if a star

appears fainter, other stars near it may appear fainter at the same time. We call such coherent changes through parts of the field *trends*. These trends could be caused by local weather patterns such as thin cloud passages or airmass changes (Howell & Jacoby 1986; Kjeldsen & Frandsen 1992; Gilliland & Brown 1988) throughout the night. The conventional approach for trend removal is differential photometry with a *reasonable* selection of template stars near the star of interest (Young et al. 1991; Everett & Howell 2001). With the help of modern CCDs, it is not hard to select a sufficient number of bright stars as a template set. However, the de-trended results are then sensitive to the selection of template stars. If the template stars contain intrinsic variables, the determined trends will be different from the true trends. Therefore, excluding such intrinsically variable stars from template stars is essential. Furthermore, because there is no guarantee that trends are the same for all stars throughout the entire field, the template selection method should be able to handle localization of trends in large fields of wide field surveys.

In this paper, we propose a new de-trending method (hereafter PDT, for Photometric De-Trending algorithm),

* dakim@cfa.harvard.edu

which incorporates a systematic template selection algorithm that can solve the problems mentioned above and consequently shows superior de-trended results. Experiments with simulated light-curves show that PDT correctly reproduces localization.

We present details of PDT in Sec. 2. In Sec. 3, we show de-trended results for synthetic light-curves containing artificially added trends and events. In addition, comparison results with the Trend Filtering Algorithm (hereafter, TFA) (Kovács et al. 2005) are also presented. In Sec. 4, we show two examples of astronomical datasets and their de-trended results. We outline future work in Sec. 5. We summarize our conclusions in Sec. 6.

2 ALGORITHM

2.1 Outline of the PDT

One of the most widely used methods for the selection of template stars is the method that chooses as a template set a sufficient number of bright stars that are not saturated, not overlapping and not at the edge of the field. Some of these bright stars could have intrinsic variability (e.g. variable or flare stars). If we avoid those stars in the selection of template set, the de-trended results will be improved. Ideally, standard stars such as Landolt standard stars (Landolt 1992) could be useful as template set. However, there are not many standard stars in the field (even in the wide field surveys). Thus, one needs to choose template stars from the field, where a few % of stars are varying (see for example Paczynski & Pojmanski 2000; Everett et al. 2002).

If the light-curve of a star manifests a trend without being intrinsically variable, then the light-curve should be highly correlated with many other light-curves of stars in that field. If a star has both trend and intrinsic variability, the light-curve of the star would not be as highly correlated with other light-curves. Therefore, a light-curve which has strong correlation with many other light-curves is a good template candidate. Our approach to the selection of template stars is to choose highly correlated subsets of stars using the similarity matrix C , in which the elements C_{ij} are the Pearson correlation values between light-curves of star i and star j .

The Pearson correlation values can be calculated by the following equation:

$$C_{ij} = \frac{1}{n-1} \frac{\sum_{t=1}^n (L_i(t)L_j(t)) - n\bar{L}_i\bar{L}_j}{\sigma_i\sigma_j}, \quad (1)$$

where $L_i(t)$ is the flux of star i at time t , n is the total number of measurements, \bar{L}_i is the mean flux of $L_i(t)$ and σ_i is the standard deviation of $L_i(t)$. The number of measurements n for every light-curve should be the same.

Using the similarity matrix and a hierarchical tree clustering algorithm explained below, we can extract multiple subsets of template stars; each subset is relatively highly correlated within itself but not with any other subsets. We call the subsets *clusters*. For each extracted cluster, we determine one representative trend light-curve by the weighted sum of all light-curves from that cluster. To remove the

trends from all light-curves, we minimize the residuals between each light-curve and the determined trends by minimizing the root mean square (rms) r_i ,

$$r_i = \sqrt{\frac{1}{n} \sum_t \left[L_i(t) - \lambda_i - \sum_k \beta_{ik} T_k(t) \right]^2}, \quad (2)$$

where n is the total number of measurements, $T_k(t)$ are the determined trends for cluster k , m is the total number of clusters, β_{ik} and λ_i are free parameters to be calculated for each light-curve. For more details about the minimization process, see Sec. 2.3.

Sometimes such minimization approaches remove not only trends, but also the intrinsic signals because one can adjust the free parameters such that the summed trends resemble the signals. This side effect is more significant when there are more free parameters to be adjusted. Therefore, PDT, which identifies one representative trend per cluster and thus has a small number of free parameters, is better suited for de-trending light-curves, especially where the rms contribution from the intrinsic signal is significant. This contrasts with TFA or similar methods that assign one free parameter per template star per individual light-curve.

In the following sections, we explain how we use the similarity matrix to choose the clusters and how we de-trend light-curves using the selected clusters.

2.2 Selection of Clusters of Light-Curves

First, we summarize traditional clustering algorithms and their shortcomings in Sec. 2.2.1. We then explain a selection method for choosing clusters of light-curves using a hierarchical tree clustering algorithm, which is more suitable than other clustering algorithms. The selection method consists of two processes. The first step is the construction of a hierarchical tree according to the similarity matrix, explained in detail in Sec. 2.2.2. The second step is the extraction of clusters from the constructed hierarchical tree using the normality test explained in Sec. 2.2.3.

2.2.1 Clustering Algorithms

In order to extract clusters of template stars, we first group stars using a clustering algorithm based on the similarity matrix. Clustering algorithms are useful for grouping large data according to their similarities (Jain et al. 1999).

We have examined several clustering algorithms, such as density-based clustering (Ester et al. 1996), K-mean (Hartigan & Wong 1979), K-medoids (also known as Partitioning around Medoids or CLARANS, Ng & Han 1994) (hereafter K-methods) and a hierarchical tree clustering algorithm (Jain et al. 1999). These algorithms first define distances between each element (light-curves in our case) and then group elements that are similar to each other based on the distance. For all our testing, we used a distance matrix in which the elements are defined as:

$$D_{ij} \equiv 1 - C_{ij}, \quad (3)$$

where C_{ij} are the Pearson correlation values between two

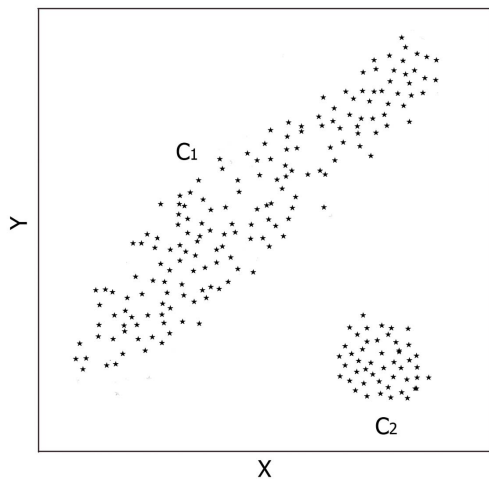


Figure 1. Conceptual illustration of the problem with most clustering methods applied to de-trending. Using most algorithms, two clusters in the figure can be easily identified. Even though some of the elements in cluster C_1 are far from each other, they are identified as one cluster. The x and y-axes indicate the distances between pairs of elements.

elements i and j , as shown in equation 1. More correlated, or more similar elements have shorter distances between them.

In choosing template sets, it is important while grouping elements that every element in the same cluster is similar to the others in the cluster. However, some of the clustering algorithms (Hartigan & Wong 1979; Ester et al. 1996; Ng & Han 1994) group into clusters elements which are not pairwise similar. This is a critical disadvantage because we would like to identify only stars that are strongly correlated to one another. Fig. 1 conceptually illustrates the problem. The x and y-axes indicate the distances between pairs of elements, where closer elements are more similar. By means of these clustering algorithms, one can easily identify the two clusters, C_1 and C_2 , in Fig. 1. Yet, some elements in the cluster C_1 are not close to other elements in the same cluster because the cluster C_1 is stretched along the diagonal direction. For example, the bottom left elements are far from the top right elements, even though they are in the same cluster. With the exception of the hierarchical tree clustering algorithm, the clustering methods mentioned above suffer from these disadvantages.

Note that the term ‘cluster’ in this paper is not used in the conventional way, where C_1 in Fig. 1 would be considered as a cluster. In the rest of paper, we will be using the term ‘cluster’ to designate ‘zone of influence’ which means a group of strongly correlated elements. In this concept, C_1 would be split into several smaller sub-groups.

2.2.2 Hierarchical Tree Clustering Algorithm

A hierarchical clustering algorithm is substantially different from density-based clustering or K-methods. It constructs a hierarchical tree by linking all elements together under the same root according to predefined distances (see equation 3). During the construction, it does not need to estimate initial

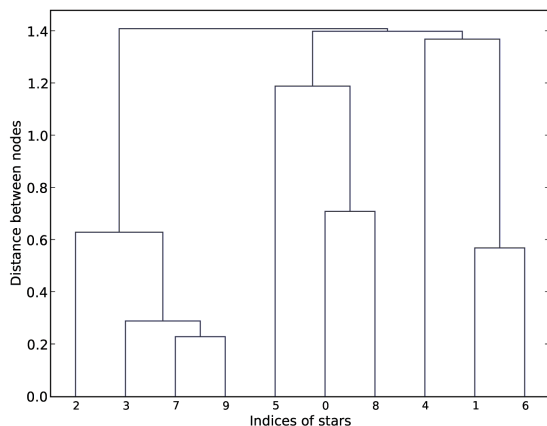


Figure 2. An example of a dendrogram. The x-axis is the index of the star, and the y-axis is the distance between nodes.

parameters such as the minimum number of elements (as in density-based clustering algorithms) or the total number of clusters (as in K-methods). This is an advantage of the hierarchical algorithm.

The constructed hierarchical tree is traditionally represented by a dendrogram as shown in Fig. 2. We use the predefined distance matrix in order to link elements and generate the dendrogram. At each stage of linkage, the algorithm joins the two closest nodes into a new set. The ‘node’ can consist of either a single element or previously connected multiple elements. This process continues until all elements belong under the same root. During this linkage process, we need to define the distances between two nodes as well. There exist several methods to calculate the distance between nodes (Jain et al. 1999). Among these methods, we use the complete-linkage method to construct the tree. In the complete-linkage method, the distance between two nodes is defined as the longest distance among the pairwise distances between the elements (as defined in equation 3) of the two nodes. Therefore, the distance between any two elements in two nodes is always smaller or equal to the distance between two nodes. The complete-linkage method was chosen because it produces more tightly bound clusters and hierarchies than other methods such as the single-linkage method (Jain et al. 1999).

Fig. 2 shows an example of a dendrogram of a hierarchical tree constructed by the complete-linkage method. We plot only 10 elements in Fig. 2 as an example. The x-axis is the index of each star and the y-axis is the distance between nodes. The height of the horizontal lines in the dendrogram represents the distance between two nodes linked together. We used the PyCluster library (de Hoon et al. 2004) to generate the hierarchical tree and the hcluster library to draw the dendrogram.

Traditionally, hierarchical algorithms do not produce clusters, unlike the other clustering algorithms that group elements into resulting clusters. This is a conventional feature of hierarchical algorithms (Daniels & Giraud-Carrier 2006) and it means that users must decide which elements

in the tree should be grouped into resulting clusters. This is equivalent to defining the number of clusters in K-means clustering or defining the connectable distance in the density based clustering. To solve this problem, we propose an extension to the hierarchical algorithm, shown in the following section, that can extract the resulting clusters from the tree without the need of predefining such parameters.

2.2.3 Agglomerative Merging Algorithm for Selection of Clusters

With the constructed dendrogram in hand, we can link every star according to the distance matrix. We now need to extract subsets of stars that are highly correlated among themselves for a template set and to exclude outliers such as intrinsic variables that can be harmful for de-trending. Furthermore, if there exist multiple and different trends in data, we should be able to separate them as well. The traditional method to achieve this is to set a certain distance value and extract subsets such that the farthest distance between elements in the subset is smaller than the set distance (e.g. subset [3, 7, 9] will be extracted given a set distance = 0.4 in Fig. 2). On the other hand, it is not easy to choose a set distance, especially for different datasets, for example with data observed under different weather conditions, different dates, or with different telescopes. As we mentioned in previous section, this is a conventional feature of the hierarchical tree algorithm in extracting relevant and representative clusters.

To alleviate this problem, we developed an agglomerative merging algorithm (bottom-up merging algorithm) to identify the clusters in the constructed tree, based on the assumption of normal distribution (Kim & Shevlyakov 2008).

First, we note that distances between correlated light-curves follow a skewed distribution in contrast to the distribution of distances of uncorrelated light-curves that is known to follow a normal distribution.

Second if one applies Fisher's transformation (Fisher 1915),

$$C'_{ij} = \frac{1}{2} \log \frac{1 + C_{ij}}{1 - C_{ij}}, \quad (4)$$

to the correlation values C_{ij} , the resulting transformed C' 's are approximately normally distributed (Anderson 1996).

Now we can claim that if a single cluster comprises correlated light-curves and does not contain outliers, the transformed distances between the light-curves in the cluster are normally distributed. We then extract subsets by merging the two closest nodes that have the shortest distance in the tree (see details of the process below). We repeat the merging processes and test the normality at every merging step to decide whether to stop the merging processes. To test normality, we use the Anderson-Darling test (Anderson & Darling 1952; Stephens 1974) which tests the null hypothesis that a dataset comes from the normal distribution. In other words, the test can statistically quantify how far the dataset departs from the normal distribution. Based on the test, one can derive the p-value that indicates the level of significance of the departures from normal distribution (D'Agostino & Stephens 1986). If the subset fails the normality test, it is inferred that there exist outliers in the subset or the subset

consists of two or more different trends. Therefore, we stop the merging process below the level where the normality test fails. If we repeat this process for extracting subsets in the hierarchical tree, we can finally obtain multiple clusters of trends without outliers.

Realistically, there is a mixture of various noise sources including Poisson noise and trends, and thus the distances between light-curves in a cluster might not be perfectly normally distributed even after Fisher's transformation. Also, because the correlation coefficients in a given cluster are not totally independent (e.g. C_{12} and C_{13} are not totally independent of C_{23}), and because we repeat the p-value testing on the same subset multiple times, the p-value should be considered as a tuning parameter (threshold) instead of its strict statistical definition. Nevertheless, using the normality test, we can extract strongly correlated elements that are placed in the central part (peak) of the distribution. Note that only strongly correlated elements are important to determine trends.

We describe the details of the agglomerative merging algorithm here:

- (i) Select initial cluster seeds to be all nodes which consist of only two elements in the constructed tree (e.g. [7, 9], [0, 8] and [1, 6] in Fig. 2).
- (ii) Define C_{seed} to be the node that has the shortest distance between two elements among selected cluster seeds from step (i).
- (iii) Merge C_{seed} with its next linked node in the tree and call it C_{merge} . If the number of elements in C_{merge} is smaller than 5, keep merging with the next linked node. This is because if the number of elements in C_{merge} is too small, the normality test would not be reliable.
- (iv) Apply the Anderson-Darling test to the distance list of C_{merge} and derive the p-value.¹ The distance list is the list of all distances between members of C_{merge} . For instance, if the indices of members in C_{merge} are [1, 2, 3], the distance list is [D_{12}, D_{13}, D_{23}] where D_{ij} is the distance matrix we defined in equation 3. We apply the Fisher's transformation before we apply the normality test as we mentioned above.
- (v) If the calculated p-value is bigger than 0.1, which means we cannot reject the null hypothesis that the distribution is normal with the significance level of 10%, set C_{merge} as new C_{seed} and go to step (iii). Otherwise, stop the merging process and go to step (vi).
- (vi) Identify C_{seed} as cluster candidate. Go to step (ii) and choose the next closest pair. Keep these processes until there remain no initial cluster seeds.
- (vii) Remove duplicated clusters from the candidates list derived at step (vi). The duplication can happen when there exist multiple seeds in one cluster, that can yield identical clusters. Note that as long as the initial cluster seeds defined in step (i) are the same, the resulting clusters are the same no matter which cluster seed we start from.
- (viii) Remove clusters whose number of elements are smaller than 10. We need a sufficient number of elements (light-curves) to cancel out the uncorrelated noise in the light-curves while determining master-trends (see Sec. 2.3).

¹ We use R statistical packages and RPy library to calculate the p-value.

(ix) Define the list of clusters from step (viii) as C_k , where k is the index of each cluster.

The clusters identified by the algorithm above are used to determine trends which we explain in the following section.

While testing the merging algorithm, we observed that if we constrain the initial seeds at step (i), we can improve our algorithm by 1) decreasing CPU processing time and 2) removing relatively contaminated clusters by other noise sources such as Poisson noise. We explain the details below.

If we select the initial seeds to be just the pairs of elements whose distances are smaller than the average value of the distance matrix (\bar{D}) at step (i), we obtain a smaller number of seeds that are more highly correlated. \bar{D} is given by:

$$\bar{D} = \frac{1}{N(N-1)} \sum_{i=1}^{N-1} \sum_{j=i+1}^N D_{ij}, \quad (5)$$

where N is the total number of light-curves. The benefit is that we speed up the algorithm by reducing the number of iterative processes that mainly consist of merging nodes and testing for normality. As we explained above, we repeat the merging and the normality test for every initial seed. Therefore, if there are fewer initial seeds, there are fewer iterative processes, thus reducing the CPU processing time. Moreover, we can remove pairs of faint stars in advance from initial seeds. Faint stars suffer from noise more than bright stars, therefore, the clusters derived with pairs of faint stars are less suited to determine trends than the clusters derived with pairs of bright stars. Note that if we use a looser constraint ($\gg \bar{D}$) and thus have too many seeds, the number of weakly correlated clusters and the computational cost will increase. On the contrary, if we use a tighter constraint ($\ll \bar{D}$) and thus fewer initial seeds, we may miss real clusters. We empirically found that any cutting values from $\bar{D}/10$ to \bar{D} give reasonable results. Within this range, the overall characteristics of the determined trends using the resulting clusters were almost identical.

In addition, it is known that the square root of the variance of correlation coefficients are generally:

$$\sigma = \frac{1 - C_{ij}^2}{\sqrt{n}}, \quad (6)$$

where C_{ij} is the correlation value between two variables and n is the total number of measurements (Bowley 1928; Hotelling 1953; Ghosh 1966). If the light-curves consist of random fluctuations (e.g. pure Poisson noise), $C_{ij} \simeq 0$. Thus, equation 6 changes to:

$$\sigma \simeq \frac{1}{\sqrt{n}} \quad (7)$$

We remove all initial seeds from step (i) whose distances are larger than $1 - 3 * \sigma$ because resulting clusters using these initial seeds would contain light-curves of mainly random fluctuation that are not correlated with other light-curves. Note that this criterion is different from the one above. For example, this occurs when there is a set of light-curves of random fluctuations. In that case, \bar{D} is ~ 1 and several initial seeds whose distances are smaller than 1 would pass the \bar{D} criteria.

We also tested another threshold cut which constrains elements in each cluster to be highly correlated. If a distance between any two elements in a given subset is bigger than \bar{D} , we stopped the merging process even if the subset was not rejected by the normality test. Nevertheless, we empirically found that resulting clusters and de-trended light-curves are not affected by this threshold.

2.3 Determination and Removal of Trends

With the extracted single or multiple clusters, we next determine the trends for each cluster (hereafter, master-trends), from the weighted sum of the cluster members as:

$$\begin{aligned} T_k(t) &= \frac{\sum_{i=1}^{N_k} w_i f_i(t)}{\sum_{i=1}^{N_k} w_i}, \\ f_i(t) &= \frac{L_i(t) - \bar{L}_i}{\bar{L}_i}, \\ w_i &= \frac{1}{\sigma_{f_i}^2}, \end{aligned} \quad (8)$$

where σ_{f_i} is the standard deviation of f_i , N_k is the total number of template stars in the cluster C_k , t is the time index with the total n measurements, $L_i(t)$ is the light-curve of i^{th} template star and \bar{L}_i is the mean value of $L_i(t)$.

This master-trend set, $T_k(t)$, is used to de-trend the individual light-curves. Each master-trend well represents the characteristic of each cluster because all the light-curves in each cluster are selected to be strongly correlated. Note that we determine just one master light-curve per cluster.

After we determine the master-trends, we remove the trends from each individual light-curve. First we normalize each light-curve $L_i(t)$ as:

$$\hat{L}_i(t) = \frac{L_i(t) - \bar{L}_i}{\bar{L}_i}. \quad (9)$$

We then assume that each light-curve $\hat{L}_i(t)$, is a linear combination of the determined master-trends $T_k(t)$, and noise, $\epsilon_i(t)$,

$$\hat{L}_i(t) = \sum_{k=1}^m \beta_{ik} T_k(t) + \epsilon_i(t), \quad (10)$$

where i are the indices of individual light-curves to be de-trended, k are the indices of master-trends, m is the total number of master-trends and β_{ik} are free parameters to be determined by means of minimization of $\sum_t \epsilon_i(t)^2$ (equivalent to minimizing r_i^2 in equation 2).

During the minimization of $\sum_t \epsilon_i(t)^2$, there is one more complication we have to consider. Let us assume there exists a single trend where flux increases monotonically and an intrinsic variable star where flux decreases monotonically. Even though the direction of the trend is different from that of the variable star, the minimization method will eventually reduce the intrinsic signal because the free parameters

can take negative values and thus minimize $\sum_t \epsilon_i(t)^2$. To eliminate this undesirable effect, we constraint the free parameters β_{ik} , to be always bigger than or equal to zero using quadratic programming (Goldfarb & Idnani 1983).²

3 TEST WITH SYNTHETIC LIGHT-CURVES

We present here the results from several simulations we performed. First, we describe the method by which we parameterized trends and how we built the simulation (see Sec. 3.1). Next, we present de-trended results of artificially inserted transits and eclipsing binaries using PDT (Sec. 3.2) and comparison results with TFA (Sec. 3.3). Finally, we show simulations and results from other unique configurations (Sec. 3.4).

3.1 Data Description

We generated ~ 500 artificial light-curves, each having different flux and 360 one-minute-exposures. During this simulation, we set x-coordinates of stars as altitude and y-coordinates as azimuth. CCD size was set to 2048x2048. The magnitudes of the stars were chosen from the USNO B1.0 catalog (Monet et al. 2003) within a particular patch of the sky (3 deg^2) [$4^h 48^m 00^s$, $20^\circ 46' 20''$] and ranged from ~ 6 mag to ~ 13 mag. Poisson noise was added to light-curves with standard deviation values (σ) set to vary from 0.001 mag to 0.02 mag. Although there exist other possible sources contributing to the noise budget such as CCD overscan, bias, dark, flat-field, etc. (Gilliland & Brown 1988), we did not include those noise sources because trends are predominantly due to weather (sky background). Bias and other such error sources are usually stable during a night observation and not a major source of trends. The results of this simulation would not be affected by such noise, as can be seen from the analysis presented in Sec. 4, where we used non-simulated data that contain bias, etc.

We added three transit signals (Mandel & Agol 2002) into three different light-curves with $\sigma = 0.01$ mag. Transit depths were 0.015, 0.020 and 0.025 mag with 60 minutes duration (one-sixth of total observation duration). We placed the transit signals at the central part of the light-curve. We also added two eclipsing binaries into two light-curves with $\sigma = 0.01$ mag. The remaining stars were set to have no intrinsic variability.

To add trends, we artificially generated four types of trends:

(i) first order atmospheric extinction. This is the typical extinction that linearly depends on the airmass: $a M_i(t)$, where a is the extinction coefficient, which is ~ 0.16 for the V and ~ 0.1 for the R band (Stalin et al. 2008), $M_i(t)$ is the

airmass of i^{th} star and is given by:

$$\begin{aligned} M_i(t) &= \sec(z_i(t)) , \\ z_i(t) &= 90^\circ - [(c + dt) + e \hat{y}_i] , \end{aligned} \quad (11)$$

where c is the starting altitude of the field ($c = 45^\circ$), d is the change of altitude per minute ($d = 0.25^\circ \text{ min}^{-1}$), e is the field of view ($e = 3 \text{ deg}^2$), $\hat{y}_i = y_i/D_y$ is the y-position of i^{th} star normalized by y-size D_y of CCD plane and t is the observational time in minutes.

To change airmass with time, we changed the altitude of the field from -45° , passing through 90° , to 45° .

(ii) position-dependent and time-dependent trend. We model this type of extinction to imitate stationary ‘clouds’ and thus to depend on the azimuthal position of the star and observation time as: $b \hat{t} \hat{x}_i$, where b is the maximum depth (for this simulation we use $b = 0.01$ mag), $\hat{t} = t/t_{\text{TOTAL}}$, is the normalized time over the total observation duration (t_{TOTAL}), $\hat{x}_i = x_i/D_x$ is the x-position of i^{th} star normalized by D_x , the x-size of CCD plane. Such position-dependent and time-dependent trends can be caused by thin cloud, Moon light or occasionally by CCD noise.

(iii) localized trend. This is an artificially CCD-localized trend that has a simple linear time dependance, $\zeta_i(t)$, given by:

$$\begin{aligned} \zeta_i(t) &= f \hat{t} , \\ f &= \begin{cases} 0.25 & x_i > 1500 \quad \text{and} \quad y_i < 500 \\ 0 & \text{otherwise} \end{cases} \end{aligned} \quad (12)$$

where x_i is the x-position of i^{th} star, y_i is the y-position of i^{th} star and \hat{t} is the normalized time as explained above. Such localized trends can be caused by non-uniform clouds or the non-uniform illumination structure of CCD images.

(iv) the second order atmospheric extinction. This is the other atmospheric extinction related to the star color, $w r C M_i(t)$, where w is proportional to the square of the optical bandwidth, C is a color index and r is the difference between the extinction coefficients in the corresponding bands (Young et al. 1991). The coefficients w and r are constant and same for all stars in the field. Even if the airmass changes for two stars are same during observation (e.g. two stars at same altitude), trends could be different due to the differences in colors (typically a few milli-magnitude differences in light-curves, Young et al. 1991). We will ignore this term until Sec. 3.4.1.

Fig. 3 shows two distinctive trends build on two bright stars. The top panel is a light-curve of a bright star which consists of the first trend, the second trend ((i), (ii)) and Poisson noise. The bottom panel is a light-curve of another bright star which consists of the first trend, the second trend, the third trend ((i), (ii), (iii)) and Poisson noise.

3.2 Identification of Clusters of Template Stars

We applied PDT to test its ability to properly identify the inserted artificial trends. Using PDT, we identified four different clusters in the dataset as shown in Fig. 4. The x and y-axis of Fig. 4 are the x and y-coordinates of the template stars on the CCD plane. Different symbols indicate different

² Quadratic programming is a mathematical optimization method which minimizes (or maximizes) a quadratic function of several unknown parameters which is subordinate to linear constraints on the parameters. We use R statistical packages to implement quadratic programming.

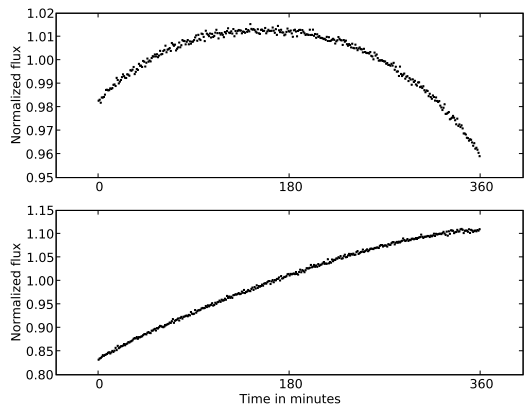


Figure 3. Two sample synthetic light-curves of two bright stars which contain trends. The light-curve at the top panel consists of the first order atmospheric extinction, position-dependent and time-dependent trend, and Poisson noise. The light-curve at the bottom panel contains an additional trend that is artificially localized CCD-localized.

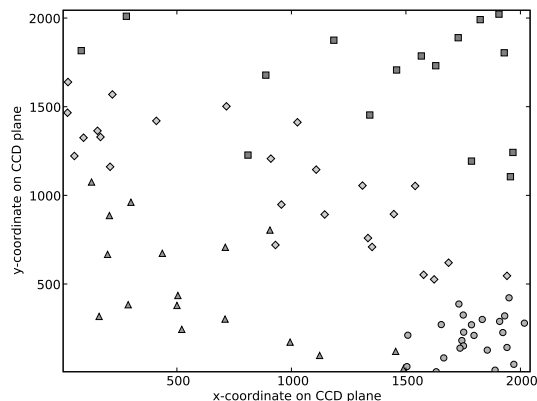


Figure 4. Positions of the identified four clusters in the artificially generated dataset. x(y)-axis is the x(y)-coordinates of stars on the field. Four different shapes mean four different clusters.

clusters. Each cluster is well separated along the y-axis due to the artificially inserted airmass ((i), $a M_i(t)$). Also, the clusters show a slope along the field due to the second trend ((ii), $b \hat{t} \hat{x}_i$). Finally, PDT exactly identified a cluster of localized trend ((iii), $\zeta_i(t)$, marked as circles in Fig. 4). As the results clearly indicate, PDT can identify and group light-curves according to their similarity, even though multiple trends are mixed together and the trends are contaminated by other noise sources such as Poisson noise.

The identified clusters do not contain any stars which are intrinsically variable (three transits and two eclipsing binaries). This shows that our clustering algorithm is also effectively excluding such unwanted outliers.

3.3 De-trending Results and Comparison with TFA

Here we compare our results to TFA. TFA is one of the particularly successful de-trending methods (Kovács et al. 2005; Tamuz et al. 2005) and it is used by exo-planet searches such as HATNet (Bakos et al. 2004). It is therefore a good comparison algorithm for our de-trending algorithm. TFA uses a large number of bright stars as a template set while excluding the light-curve being de-trended. TFA does not eliminate potentially dangerous stars, such as the stars which have intrinsic variability, from the template set, and it assigns one free parameter per template light-curve. In contrast, our algorithm can automatically exclude such intrinsically variable stars and assign one free parameter per cluster of template light-curves.

First, we present the de-trended results of three transit signals. The top panel of Fig. 5 shows the raw light-curves before any de-trending treatments. Each column shows three different transits with different depth (0.015, 0.020 and 0.025 mag from left to right). TFA results are shown in the middle panel of Fig. 5, while PDT results are shown in the bottom panel. We used 60 bright stars as a template set for TFA. We excluded the three transits light-curves from the template set because in realistic scenarios, it is uncommon for there to be three transit events occurring in the same field and same epoch. However, we did not exclude the two eclipsing binaries from the template set for TFA because variable stars such as eclipsing binaries are common in the field. As the middle panel shows, TFA suppressed each transit signal more than PDT. The suppression was mainly caused by the presence of the eclipsing binaries in the template set. Because TFA tries to minimize the residual between the target light-curve to be de-trended and a linear combination of light-curves from the template set that might contain intrinsic variables such as the two eclipsing binaries in this simulation, it occasionally suppresses the intrinsic signals of the target light-curve by removing any similar signals between the target light-curve and the template set. In contrast, results from PDT, which can select template sets that do not contain the three transits or the two eclipsing binaries, show less significant signal depression and clearer transit signals than TFA results (see bottom panel of Fig. 5).

Note that one of the eclipsing binaries was phased to the transits to show signal depression effect of TFA. Such coincidences are not common, but we cannot ignore the probability especially in the case of wide field surveys which simultaneously monitor more than several hundred stars. If we exclude the eclipsing binary from the template set, the de-trended results using TFA are almost identical to the results using PDT.

We performed χ^2 tests comparing de-trended results and original transit signals for all three transits to check how successfully both de-trending algorithms regenerated the intrinsic signals. Table 1 shows individual χ^2 values of each transit and χ^2 ratios of TFA to PDT. The χ^2 ratio is defined as $\chi^2_{\text{TFA}}/\chi^2_{\text{PDT}}$. Therefore, if the χ^2 ratio is bigger than one, it means that PDT results are more similar to the original transit signals than TFA results. As Table 1 shows, all three χ^2 ratios are slightly bigger than one.

If the rms contribution from intrinsic signal is significant, such as the two eclipsing binaries in this simulation,

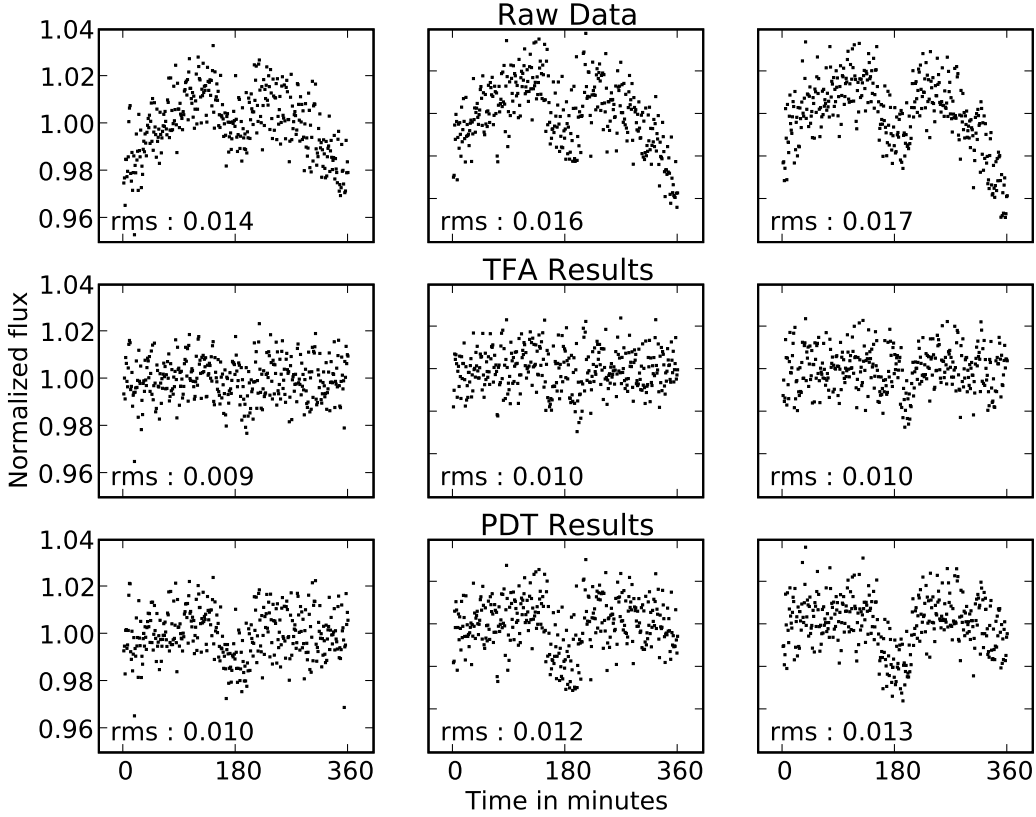


Figure 5. De-trended results of the simulated three transit events. Each column represents each different transit depth of 0.15, 0.20 and 0.25 mag from left to right. The top panel is raw light-curves. The middle panel is TFA results, and the bottom panel is PDT results. We indicate the rms of each light-curve as well.

Table 1. χ^2 values of each transit and χ^2 ratio of TFA to PDT

Transit depth	TFA	PDT	χ^2 ratio
0.015	1.08	1.03	1.05
0.020	1.49	1.39	1.07
0.025	1.69	1.50	1.13

any method which minimizes the rms to de-trend light-curves will dilute the intrinsic signals. This is the critical problem of the rms minimization algorithm and cannot be perfectly overcome as long as we use the minimization approach. One solution to reduce this side effect is to decrease the number of free parameters (see Sec. 2) and constraint the free parameters to be bigger than or equal to zero (see Sec. 2.3). PDT, by construction, has fewer parameters than TFA because we determine one master-trend per one cluster. Also, PDT can constraint the free parameters using quadratic programming.

Fig. 6 shows the de-trended results of the two eclipsing binaries by both TFA and PDT. The top left panel is the raw light-curve of one eclipsing binary affected by all three

trends including localized trend (trend (iii)) and thus the average flux of the light-curve is increasing along time. The top right panel is the raw light-curve of another eclipsing binary affected by only two trends (trend (i) and trend (ii)) and thus it does not show increase of flux because the intrinsic signal is relatively bigger than the two trends. The middle panel is the TFA results, and the bottom panel is the PDT results. In both cases, TFA not only removed the trends but also diluted the intrinsic signals. In contrast, PDT removed only the trends and successfully regenerated the intrinsic signals of two binaries.

In addition, we indicate the rms of the de-trended light-curves in each panel of Fig. 5 and 6. The rms values are always smaller in TFA results than in PDT results because TFA has more adjustable free parameters than PDT has and TFA can set free parameters to be any values including negative values. However, as the de-trended results show, smaller rms do not always mean better de-trended results, especially when intrinsic signals contribute mainly to rms of light-curves such as the two eclipsing binaries.

Note the TFA has a *reconstruction* phase which can greatly improve S/N of periodic signals with the initial guess of the signal models (Kovács et al. 2005; Kovacs & Bakos 2008). Nevertheless, PDT is designed to regenerate

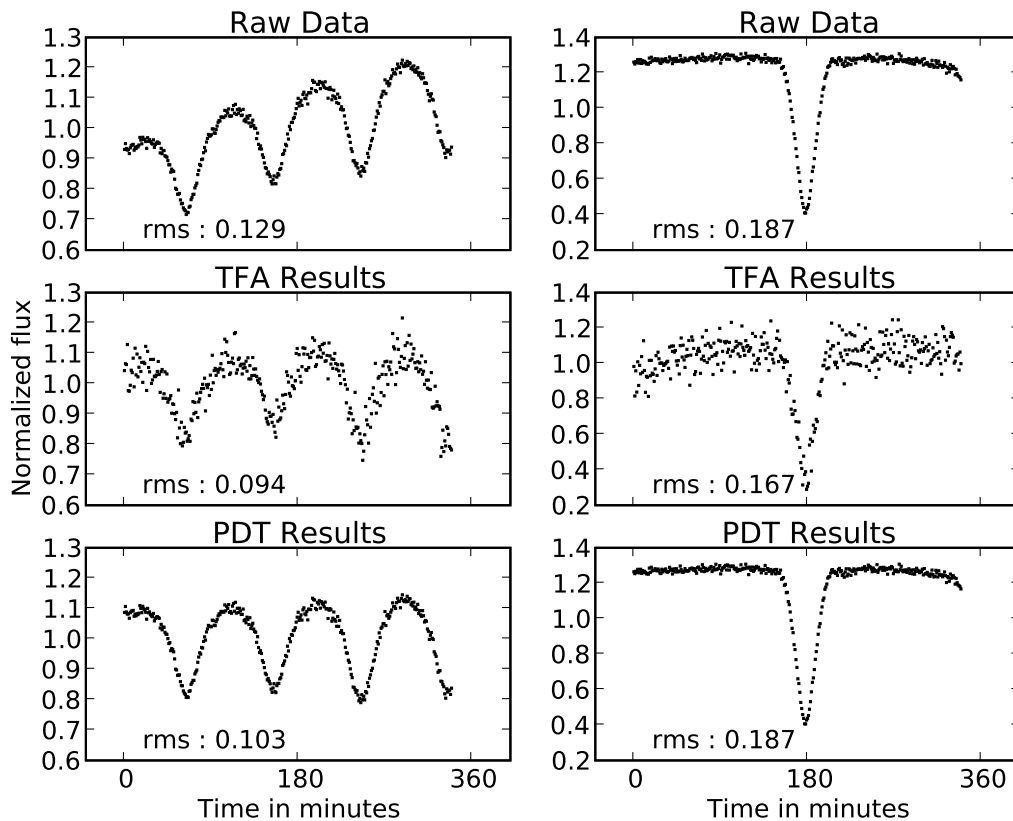


Figure 6. De-trended results of the simulated two eclipsing binaries. The top panel is raw light-curves. The middle panel is TFA results, and the bottom panel is PDT results. We indicate the rms of each light-curve as well.

any types of intrinsic signals whether they are periodic or not.

3.4 Second Order Extinction and Other Considerations

3.4.1 Second Order Extinction Test

We now turn our attention to the second order atmospheric extinction related to colors of stars ((iv) at Sec.3.1). After performing several simulations with realistic parameters (e.g. different field of view from $.1 \text{ deg}^2$ to 5 deg^2 , different bands such as B and V, different observation durations from one hour to six hours, etc) that contain both first and second order extinction, we found that PDT cannot separate clusters according to star color. The reason is that both extinctions depend linearly on airmass, and the first order extinction is much larger than the second order extinction when using realistic values for the coefficients. Therefore, PDT identifies clusters that mainly depend on the first order extinction.

It is worth mentioning that PDT can identify clusters based on colors if we isolate only the second order extinction. We performed another simulation to test this:

(i) Generate ~ 500 light-curves that contain only the second order extinction and Poisson noise. We extracted B-R

Table 2. Mean and standard deviation values (σ) of colors of stars in resulting six clusters

Cluster	mean	σ
C_1	1.40	0.11
C_2	1.39	0.17
C_3	1.18	0.27
C_4	0.87	0.15
C_5	0.79	0.09
C_6	-0.25	0.05

colors of stars from USNO B1.0 catalog within a particular patch of the sky (3 deg^2) [$4^h 48^m 00^s$, $20^\circ 46' 20''$], which is the same field of view as in the previous simulation shown in Sec. 3.1.

(ii) Apply PDT to the light-curves and identify clusters.

Table 2 shows the mean and standard deviation values (σ) of the colors of stars in clusters identified by PDT. Although some of the clusters (e.g. C_1 and C_2) could be regarded as clusters of the same trend because they have similar mean color values, PDT did a good job of separating bluish cluster (C_6) from reddish (C_1 to C_5) clusters.

3.4.2 Pure Poisson Noise Case

We tested both PDT and TFA with ~ 500 synthetic light-curves with pure Poisson noise but no trends. We also added three artificial transit events into three individual light-curves. We used 60 bright stars as a template set for TFA. Even though there were no trends, TFA still de-trended the light-curves by using the template stars, and it eventually suppressed the intrinsic signals of the transits. By contrast, PDT did not identify any clusters because we exclude clusters that consist of only Poisson noise (see Sec. 2.2.3). Consequently, it did not de-trend light-curves and thus did not suppress any intrinsic signals.

Note that Poisson noise is not always the dominant noise source in light-curves. The example referred here shows that if there are none-strongly correlated elements (trends) in dataset, then PDT will not de-trend the dataset.

4 TEST WITH ASTRONOMICAL DATASETS

We present now two examples of astronomical datasets. One is from TAOS (The Taiwan-American Occultation Survey) (Lehner et al. 2009), and the other is from an occultation survey using Megacam on the 6.5m Multi-Mirror Telescope (MMT) (Bianco et al. 2009). Both examples show multiple trends that are well localized on the CCD plane. Such localization of trends could be caused by various noise sources such as airmass, cloud passages, noise of CCD images, telescope vibration, defects of photometry and so on. These localizations often happen with wide field observations.

4.1 An Example of TAOS Dataset

The scientific goal of TAOS (Zhang et al. 2008) is to detect km-sized Kuiper Belt Objects (Luu & Jewitt 2002) at a distance of Neptune or beyond. TAOS data usually suffer from low S/N and systematic trends due to the small telescope size (four 50cm telescopes), noise of CCD images, defects of photometry and unstable local weather (e.g. cloud passages). The field of view of the TAOS telescopes is 3 deg^2 and the sampling rate is 5 Hz. We chose one sample set of light-curves generated by the TAOS photometry pipeline (Zhang et al. 2009) and de-trended the light-curves using PDT. The total observation time of the light-curves was 1.5 hours.

Fig. 7 shows the determined master-trends and examples of de-trended light-curves. The top left panel shows the position of stars in identified clusters on the CCD plane. Different shapes indicate different clusters. The clusters are localized on the CCD plane due to unstable local weather, noise of CCD images and defects of photometry. The bottom two panels show example light-curves of two non-variable stars. The upper light-curves of the two bottom panels are before de-trending and the lower light-curves are after de-trending. As the results show, PDT removed trends from both light-curves.

4.2 An Example of Megacam Dataset

We also applied PDT to a dataset obtained using Megacam (McLeod et al. 1998) at the MMT at Mount Hop-

kins, Arizona. Megacam is a mosaic CCD which consists of 36 chips. The size of each CCD is 2K by 4K and the field of view is $24' \times 24'$. Megacam was used in *continuous-readout* mode achieving 200Hz sampling rate in order to detect stellar occultations caused by Kuiper Belt Objects (Bianco et al. 2009). Due to the high sampling rate, telescope vibrations, defects of photometry and the readout technique, these Megacam data show strong trends. The total observation time of the selected dataset was 15 minutes.

The top left panel of Fig. 8 shows the position of stars in identified clusters. Different shapes indicate different clusters. The top right panel shows the determined master-trends. We magnified a part of the light-curves (~ 5 seconds) to clearly show the trends. The bottom two panels show two example light-curves of non-variable stars before and after de-trending.

As the figure shows, two clusters marked as circles and triangles are localized on the CCD plane. In our analysis, we found that often the clusters were divided along the horizontal half divide (e.g. clusters marked as circles and triangles in Fig. 8), and that can be attributed to details of the readout mode, but we also found cases where the clustering that crossed over the horizontal divide (e.g. a cluster marked as squares in 8). The trends are likely due to a combination of weather patterns, photometry and the way the CCD was read out (Bianco et al. 2009).

5 NOTES AND FUTURE WORK

A weakness of PDT is that it cannot remove trends that are manifested in just a few light-curves and are not highly correlated. For example, moving asteroids or satellites could result in an increase and decrease of the estimated flux of a few background stars in the neighborhood of the track. These trends are out of phase throughout the light-curves because the asteroids or satellites are moving across the field. For these reasons, strongly trended light-curves are not highly correlated and thus PDT cannot group them into clusters. We are planning to handle this phase-shift of trends in a future version of PDT.

We are also applying PDT to astronomical datasets, e.g. TAOS and MMT, in order to detect various transient events such as KBO occultations, flare stars, micro-lensing events and exo-planet transits.

6 CONCLUSION

In this paper, we presented the Photometric De-Trending algorithm (PDT), a new de-trending algorithm. We first determined the trends by constructing a hierarchical tree based on the similarity matrix. Elements of the similarity matrix are the Pearson correlation values of all pairs of light-curves. After that, a bottom-up merging algorithm was applied to the constructed tree in order to identify subsets of light-curves that we call clusters. At each step of the merging process, we tested the normality of the subsets and determined where to stop. By means of the normality test, we could select reliable clusters of trends. For each cluster, we determined one representative master-trend by weighted sum of the normalized light-curves. This procedure greatly

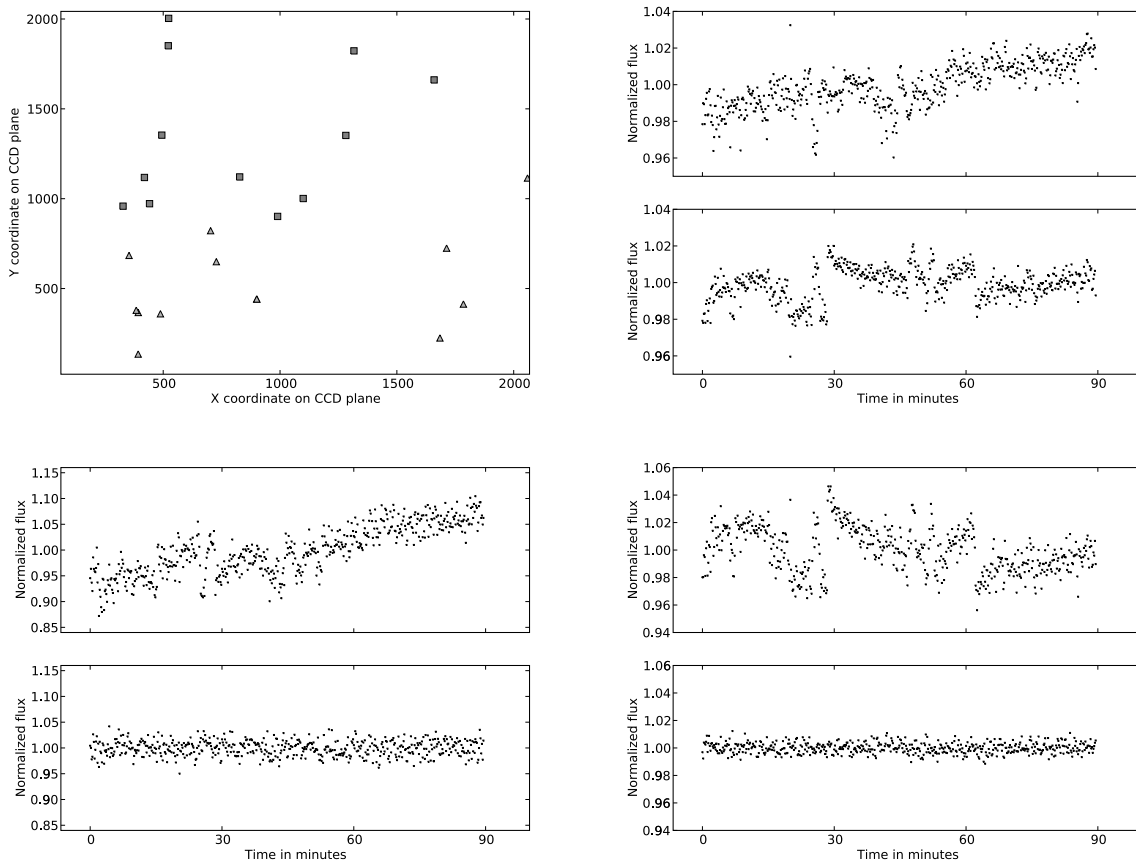


Figure 7. An example of TAOS dataset. Top left : Position of stars in identified two clusters. $x(y)$ -axis is the $x(y)$ -coordinate of stars on the CCD plane. Different shapes indicate different clusters. Top right : Determined two master-trends. Bottom left and bottom right : Two example light-curves before and after de-trending. Upper panels are before de-trending and lower panels are after de-trending.

constrained the number of free parameters to be calculated, and thus showed less significant signal depression than other de-trending algorithms such as Trend Filtering Algorithm (TFA). Finally, in order to remove the trends from individual light-curves, we used quadratic programming to minimize the residual between each target light-curve and the determined master-trends. Note that PDT is designed to remove only the fluctuations that are common among stars. If the fluctuations are unique to an individual star, the fluctuations will be preserved.

We performed several simulations of synthetic light-curves with different initial parameters such as total duration of observation, transit duration, field of view, exposure time etc, to test PDT and showed some of the simulation results in this paper.

First, we tested PDT with ~ 500 synthetic light-curves that contain the first order atmospheric extinction (air-mass), artificial trends, Poisson noise and events (three transits and two eclipsing binaries). We applied PDT to these synthetic light-curves in order to determine trends and to regenerate the inserted events. PDT successfully identified multiple clusters of different trends which were the mixture of different trends and noise. These identified clusters well represented the overall characteristic of the trends through

the field. We compared de-trended results of PDT with one another de-trending algorithm (TFA). PDT results were an improvement over TFA results, especially when 1) the dataset contains intrinsic variables that would be included in template set of TFA or 2) the rms contribution from the intrinsic signals is significant.

We also tested PDT with ~ 500 synthetic light-curves that contain color dependent second order extinction and Poisson noise. Trends appearing in light-curves can be slightly different due to differences in color. We found that PDT can identify clusters according to color. However, in realistic scenarios, it is not easy to isolate only the second order extinction because, even if one correctly removes the first order extinction for all stars, there exist other various noise sources which dilute trends caused by the second order extinction.

In the case of dataset of random fluctuations (e.g. pure Poisson noise), which does not have any trends, we do not need to de-trend the dataset. PDT can distinguish the light-curves of random fluctuations using the characteristics of the distribution of correlation coefficients. Therefore, PDT does not de-trend these light-curves and thus preserves any intrinsic signals.

Examples of two astronomical datasets are also pre-

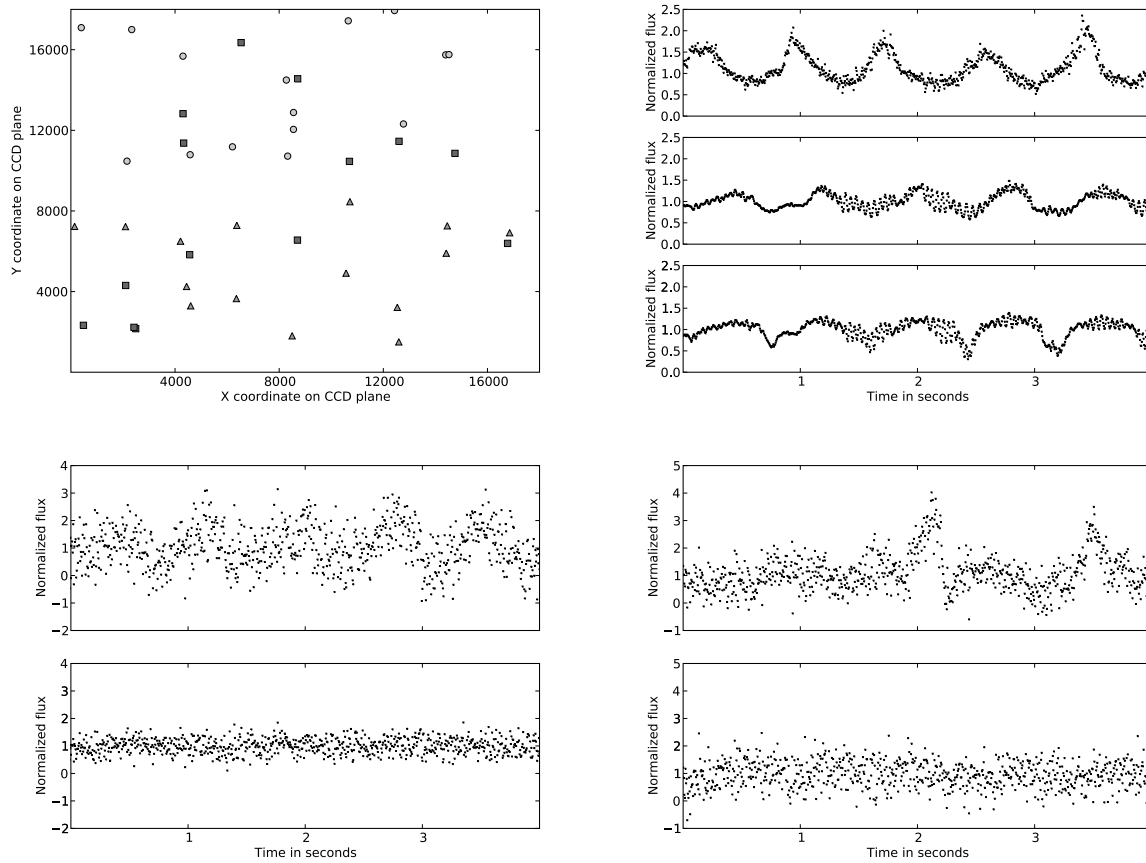


Figure 8. An example of Megacam dataset. Top left : Position of stars in identified three clusters. $x(y)$ -axis is the $x(y)$ -coordinate of stars on the CCD plane. Different shapes indicate different clusters. Top right : Determined three master-trends. Bottom left and bottom right : Two example light-curves before and after de-trending. Upper panels are before de-trending and lower panels are after de-trending.

sented. They show multiple trends in the field caused by various noise sources such as airmass, cloud passages, telescope vibration, defects of photometry and so on. PDT performed well and removed trends that appeared in the datasets.

In this paper, we show the simulation results of wide field data only. However, PDT can be applied to narrow field data as well if there are enough stars in the field (\sim a few hundreds). In addition, PDT is useful to extract global trends that can represent the overall characteristics of a dataset. The extracted trends can give a general idea of how much the data are contaminated by the trends.

The software package of PDT is provided at <http://timemachine.iic.harvard.edu>.

ACKNOWLEDGEMENTS

This work is supported by the Korea Research Foundation. Y.-I. Byun also acknowledges the grant of KRF-2007-C00020. We thank R. Reid, R. Dave, G. Wachman and D. Preston at the Harvard, Initiative in Innovative Computing (IIC), and A. W. Blocker at the Harvard University Department of Statistics for comments and suggestions on this paper. We also thank the Harvard-Smithsonian Center

for Astrophysics and IIC for providing computing facilities and research space. The simulations and the de-trending of datasets in this paper were run on the Odyssey cluster supported by the FAS Research Computing Group at the Harvard.

REFERENCES

- Akerlof C., Amrose S., Balsano R., Bloch J., Casperson D., Fletcher S., Gisler G., Hills J., Kehoe R., Lee B., Marshall S., McKay T., Pawl A., Schaefer J., Szymanski J., Wren J., 2000, *AJ*, 119, 1901
- Alonso R., Brown T. M., Torres G., Latham D. W., Sozzetti A., Mandushev G., Belmonte J. A., Charbonneau D., Deeg H. J., Dunham E. W., O'Donovan F. T., Stefanik R. P., 2004, *ApJL*, 613, L153
- Anderson T. W., 1996, *Statistical Science*, 11, 20
- Anderson T. W., Darling D. A., 1952, *Annals of Mathematical Statistics*, 23, 193
- Bakos G., Noyes R. W., Kovács G., Stanek K. Z., Sasselov D. D., Domsa I., 2004, *PASP*, 116, 266
- Bakos G. Á., Noyes R. W., Kovács G., Latham D. W., Sasselov D. D., Torres G., Fischer D. A., Stefanik R. P.,

- Sato B., Johnson J. A., Pál A., Marcy G. W., Butler R. P., Esquerdo G. A., et al. 2007, *ApJ*, 656, 552
- Bianco F. B., Protopapas P., McLeod B. A., Alcock C. R., Holman M. J., Lehner M. J., 2009, ArXiv e-prints
- Bowley A. L., 1928, *Journal of the American Statistical Association*, 23, 31
- Burke C. J., McCullough P. R., Valenti J. A., Long D., Johns-Krull C. M., Machalek P., Janes K. A., Taylor B., Fleenor M. L., Foote C. N., Gary B. L., García-Melendo E., Gregorio J., Vanmunster T., 2008, *ApJ*, 686, 1331
- D'Agostino R. B., Stephens M. A., 1986, *Goodness-of-fit techniques*. Marcel Dekker, Inc., New York, NY, USA, p. 107
- Daniels K., Giraud-Carrier C., 2006, in *ICMLA '06: Proceedings of the 5th International Conference on Machine Learning and Applications Learning the Threshold in Hierarchical Agglomerative Clustering*. IEEE Computer Society, Washington, DC, USA, pp 270–278
- de Hoon M. J. L., Imoto S., Nolan J., Miyano S., 2004, *BIOINFORMATICS*, 20, 1453
- Ester M., Kriegl H. P., Sander J., Xu X., 1996, in *Proceedings of 2nd International Conference on Knowledge Discovery and Data Mining (KDD-96) A Density-Based Algorithm for Discovering Clusters in Large Spatial Databases with Noise*. Portland, Oregon, USA, pp 226–231
- Everett M. E., Howell S. B., 2001, *PASP*, 113, 1428
- Everett M. E., Howell S. B., van Belle G. T., Ciardi D. R., 2002, *PASP*, 114, 656
- Fisher R. A., 1915, *Biometrika*, 10, 507
- Ghosh B. K., 1966, *Biometrika*, 53, 258
- Gilliland R. L., Brown T. M., 1988, *PASP*, 100, 754
- Goldfarb D., Idnani A., 1983, *Mathematical Programming*, 27, 1
- Hartigan J. A., Wong M. A., 1979, *Applied Statistics*, 28, 100
- Hotelling H., 1953, *Journal of the Royal Statistical Society. Series B (Statistical Methodology)*, 15, 193
- Howell S. B., Jacoby G. H., 1986, *PASP*, 98, 802
- Jain A. K., Murty M. N., Flynn P. J., 1999, *ACM Computing Surveys*, 31, 264
- Kim K., Shevlyakov G., 2008, *Signal Processing Magazine, IEEE*, Vol. 25, No. 2, pp 102–113
- Kjeldsen H., Frandsen S., 1992, *PASP*, 104, 413
- Kovács G., Bakos G., Noyes R. W., 2005, *MNRAS*, 356, 557
- Kovács G., Bakos G. A., 2008, *Communications in Asteroseismology*, 157, 82
- Landolt A. U., 1992, *AJ*, 104, 340
- Lehner M. J., Wen C.-Y., Wang J.-H., Marshall S. L., Schwamb M. E., Zhang Z.-W., Bianco F. B., Giammarco J., Porra R., Alcock C., Axelrod T., Byun Y.-I., Chen W. P., Cook K. H., Dave R., King S.-K., Lee T., Lin H.-C., Wang S.-Y., Rice J. A., de Pater I., 2009, *PASP*, 121, 138
- Luu J. X., Jewitt D. C., 2002, *ARA&A*, 40, 63
- Mandel K., Agol E., 2002, *ApJL*, 580, L171
- McCullough P. R., Stys J. E., Valenti J. A., Fleming S. W., Janes K. A., Heasley J. N., 2005, *PASP*, 117, 783
- McLeod B. A., Gauron T. M., Geary J. C., Ordway M. P., Roll J. B., 1998, in D'Odorico S., ed., *Society of Photo-Optical Instrumentation Engineers (SPIE) Conference Series* Vol. 3355 of Society of Photo-Optical Instrumentation Engineers (SPIE) Conference Series, Megacam: paving the focal plane of the MMT with silicon. pp 477–486
- Monet D. G., Levine S. E., Canzian B., Ables H. D., Bird A. R., Dahn C. C., Guetter H. H., Harris H. C., Henden A. A., Leggett S. K., Levison H. F., Luginbuhl C. B., Martini J., Monet A. K. B., Munn J. A., Pier J. R., Rhodes A. R., Riepe B., et al. 2003, *AJ*, 125, 984
- Ng R. T., Han J., 1994, in Bocca J., Jarke M., Zaniolo C., eds, *20th International Conference on Very Large Data Bases*, September 12–15, 1994, Santiago, Chile proceedings Efficient and Effective Clustering Methods for Spatial Data Mining. Morgan Kaufmann Publishers, Los Altos, CA 94022, USA, pp 144–155
- Paczynski B., Pojmanski G., 2000, in *Bulletin of the American Astronomical Society* Vol. 32 of Bulletin of the American Astronomical Society, Monitoring All Sky for Variability. p. 687
- Pál A., Bakos G. Á., Torres G., Noyes R. W., Latham D. W., Kovács G., Marcy G. W., Fischer D. A., Butler R. P., Sasselov D. D., Sipőcz B., Esquerdo G. A., Kovács G., Stefanik R., Lázár J., Papp I., Sári P., 2008, *ApJ*, 680, 1450
- Pigulski A., Pojmański G., 2008, *A&A*, 477, 907
- Pojmanski G., 2005, *VizieR On-line Data Catalog: J/other/AcA/50.177*. Originally published in: 2000AcA....50..177P, 50, 5001
- Pollacco D., Skillen I., Collier Cameron A., Loeillet B., Stempels H. C., Bouchy F., Gibson N. P., Hebb L., Hébrard G., Joshi Y. C., McDonald I., Smalley B., Smith A. M. S., Street R. A., et al. 2008, *MNRAS*, 385, 1576
- Schmidt E. G., 1991, *AJ*, 102, 1766
- Schmidt E. G., Langan S., Rogalla D., Thacker-Lynn L., 2007, *AJ*, 133, 665
- Stalin C. S., Hegde M., Sahu D. K., Parihar P. S., Anupama G. C., Bhatt B. C., Prabhu T. P., 2008, *Bulletin of the Astronomical Society of India*, 36, 111
- Stephens M. A., 1974, *Journal of the American Statistical Association*, 69, 730
- Szczygiel D. M., Fabrycky D. C., 2008, *VizieR Online Data Catalog*, 837, 71263
- Tamuz O., Mazeh T., Zucker S., 2005, *MNRAS*, 356, 1466
- Young A. T., Genet R. M., Boyd L. J., Borucki W. J., Lockwood G. W., Henry G. W., Hall D. S., Smith D. P., Baliumas S. L., Donahue R., Epan D. H., 1991, *PASP*, 103, 221
- Zhang Z.-W., Bianco F. B., Lehner M. J., Coehlo N. K., Wang J.-H., Mondal S., Alcock C., Axelrod T., Byun Y.-I., Chen W. P., Cook K. H., Dave R., de Pater I., Porra R., Kim D.-W., et al. 2008, *ApJL*, 685, L157
- Zhang Z.-W., Kim D.-W., Wang J.-H., Lehner M. J., Chen W. P., Byun Y.-I., Alcock C. R., Axelrod T., Bianco F. B., Cook K. H., King S.-K., Lee T., Lin H.-C., Marshall S. L., Schwamb M. E., Wang S.-Y., Wen C.-Y., 2009, In preparation